Parametric excitation of a ferrimagnetic sphere resonator

Eyal Buks*

Andrew and Erna Viterbi Department of Electrical Engineering, Technion, Haifa 32000 Israel
(Dated: December 2, 2025)

The response of a ferrimagnetic sphere resonator to an externally applied parametric excitation is experimentally studied. Measurement results are compared with predictions derived from a theoretical model, which is based on the hypothesis that disentanglement spontaneously occurs in quantum systems. According to this hypothesis, time evolution is governed by a modified master equation having an added nonlinear term that deterministically generates disentanglement. It is found that the disentanglement–based model is compatible with the experimental results. In particular, the model can qualitatively account for an experimentally observed instability in the system under study, which cannot be derived from any theoretical model that is based on a linear master equation.

Introduction – Multistability is experimentally observed in many quantum systems. In contrast, the linearity of standard quantum mechanics (QM) excludes multistability in systems having Hilbert space of finite dimensionality. In the current study, this apparent conflict is experimentally and theoretically explored by studying the response of a ferrimagnetic sphere resonator (FMSR) to an externally applied parametric excitation.

In the classical realm, the response of a resonator to an externally applied parametric excitation (longitudinal driving) is well described by the Mathieu model [1]. When the excitation frequency is tuned to a parametric resonance, above a critical value of the parametric excitation amplitude [2] the system's steady state response becomes bistable [3]. Moreover, with an added applied monochromatic forcing (transverse driving), the resonator's response exhibits dependency on the relative phase between longitudinal and transverse driving tones. This dependency can be exploited for the construction of amplifiers having a phase–sensitive gain.

In the quantum realm, similar effects can be explored using spins [4]. Longitudinal driving can be applied by modulating the magnetic field parallel to the spins' magnetization vector, whereas modulating the perpendicular component gives rise to transverse driving. The effect of parametric excitation (i.e. longitudinal driving, aka parallel pumping) applied to magnetically ordered dielectrics has been extensively studied [5]. Experimental observation of a response qualitatively similar to what is predicted by the Mathieu model has been first reported in [6]. In the region where multistability occurs, the experimentally observed spins' response becomes hysteretic.

Previously proposed theoretical explanations for experimentally observed multistabilities in finite quantum systems are based on the assumption that time evolution is nonlinear. For spin systems, nonlinearity can be introduced by implementing the Holstein–Primakoff transformation [7], which allows expressing spin operators in terms of annihilation and creation Bosonic operators. In this transformation, which is henceforth referred to as

Bosonization, the spins' Hilbert space having finite dimensionality is mapped into a space having infinite dimensionality. In the presence of magnetic anisotropy, this method gives rise to nonlinearity in the time evolution, which, in turn, enables both instability and multistability [8]. In contrast, for finite quantum systems, both instability and multistability are theoretically excluded provided that time evolutions for the systems's reduced density operator ρ is governed by a master equation that linearly depends on ρ [9].

The above–discussed difficulty to justify the Bosonization–based model, which enables multistabilities that are otherwise theoretically excluded [10], is the main motivation for the current study. Here, an alternative theoretical model, which is based on the hypothesis that disentanglement spontaneously occurs in quantum systems [11], is explored. According to this hypothesis, time evolution is governed by a modified master equation having an added nonlinear term [see Eq. (1) below]. A FMSR is used to experimentally validate the proposed model. While the impact of disentanglement on the FMSR response to transverse driving has been explored in [12], here the effect of parametric excitation is studied. It is found that the disentanglement–based model can qualitatively account for an instability, which is experimentally–observed in the system under study, and which is arguably inconsistent with any linear master equation.

Modified master equation – The spontaneous disentanglement hypothesis is based on the assumption that time evolution is governed by a master equation for the reduced density operator ρ having a form given by [11, 13–16]

$$\frac{\mathrm{d}\rho}{\mathrm{d}t} = i\hbar^{-1}\left[\rho, \mathcal{H}\right] + \mathcal{L} - \Theta\rho - \rho\Theta + 2\left\langle\Theta\right\rangle\rho , \quad (1)$$

where $\hbar$ is the Planck's reduced constant, $\mathcal{H} = \mathcal{H}^\dagger$ is the Hamiltonian, $\mathcal{L}$ is a Lindblad superoperator [17] (which linearly depends on ρ), $\Theta = \Theta^\dagger$ and $\left\langle\Theta\right\rangle = \mathrm{Tr}\left(\Theta\rho\right)$. The added term $-\Theta\rho - \rho\Theta + 2\left\langle\Theta\right\rangle\rho$ in Eq. (1) deterministically generates disentanglement. The dependency of the disentanglement operator Θ on ρ gives rise to nonlinear dynamics. The construction of the disentanglement operator Θ is explained in [11]. The disentanglement process

is characterized by a rate denoted by γ_{D}. For spin systems, the Lindblad superoperator $\mathcal{L}$ is characterized by energy–relaxation Γ_1 and dephasing Γ_φ rates, thermal occupation factor $\hat{n}_0$, and longitudinal T_1 and transverse T_2 relaxation times [see Eq. (17.154) of Ref. [18]].

Driven L spin system – The system under study is composed of L coupled spins 1/2. The total angular momentum vector operator $\mathbf{S} = (S_x, S_y, S_z)$ in units of $\hbar/2$, is given by $\mathbf{S} = \sum_{l=1}^{L} \mathbf{S}_l$, where $\mathbf{S}_l = (S_{l,x}, S_{l,y}, S_{l,z})$ is the l'th spin angular momentum vector operator. The closed-system Hamiltonian $\mathcal{H}$ is given by [12]

$$
\begin{aligned}
\frac{\mathcal{H}}{\hbar} = {} & -\frac{\omega_z S_z}{2} \\
& + \frac{\omega_{\mathrm{K}}\left(S_+ S_- + S_- S_+\right) + \omega_{\mathrm{A}}\left(S_+^2 + S_-^2\right)}{8} \\
& + \frac{S_+ \Omega_{\mathrm{T}1} e^{i\omega_{\mathrm{T}} t} + S_- \Omega_{\mathrm{T}1}^* e^{-i\omega_{\mathrm{T}} t}}{4} ,
\end{aligned}
\tag{2}
$$

where $S_\pm = S_x \pm i S_y$, the rates ω_{K}, ω_{A}, $\omega_{\mathrm{T}} = \omega_0 + \omega_{\mathrm{d}}$ (transverse driving angular frequency), ω_0 (angular resonance frequency) and ω_{d} (transverse driving angular detuning frequency) are real constants, $\Omega_{\mathrm{T}1} = |\Omega_{\mathrm{T}1}| e^{i\phi_{\mathrm{T}}}$ (transverse driving amplitude) is a complex constant, the real time–dependent angular frequency ω_z is given by $\omega_z = \omega_0 + \Omega_{\mathrm{L}1} \cos\left(2\left(\omega_{\mathrm{T}} + \omega_{\mathrm{f}}\right) t\right)$, where ω_{f} (longitudinal driving angular detuning frequency) and $\Omega_{\mathrm{L}1}$ (longitudinal driving amplitude) are real constants. The terms $S_+ S_- + S_- S_+ = 2\left(S_x^2 + S_y^2\right)$ and $S_+^2 + S_-^2 = 2\left(S_x^2 - S_y^2\right)$ in the Hamiltonian $\mathcal{H}$ (2) account for magnetic anisotropy. The following commutation relations hold $[S_i, S_j] = 2i\epsilon_{ijk} S_k$, $[S_z, S_\pm] = \pm 2 S_\pm$, and $[S_+, S_-] = 4 S_z$. Equations of motion obtained from the Hamiltonian $\mathcal{H}$ (2) (without disentanglement) are derived in section S1 of the supplementary materials (SM). Note that alternative methods to model dipolar coupling are reviewed in [19].

The two–spin case – For sufficiently small number L of spins, the effect of disentanglement can be numerically explored. Matrix representation of the Hamiltonian $\mathcal{H}$ [see Eq. (2)] for the case $L = 2$ (i.e. two spins) is derived in SM section S2. Time evolution of the magnetization $\langle \mathbf{S} \rangle$, which is derived by numerically integrating the modified master equation (1), is shown in the plot in Fig. 1. For the assumed parameters' values (which are listed in the figure caption), the Bloch sphere is divided into two basins of attraction corresponding to two locally–stable steady state solutions of the modified master equation (see the red $\times$ symbols in Fig. 1). For these two steady states $\phi_2 - \phi_1 = \pi$, where ϕ_n is the oscillation phase of the n'th steady state with respect to the externally applied parallel pumping, and where $n \in \{1, 2\}$.

This bistability, which is induced by disentanglement, resembles the above–threshold response of a parametrically driven classical resonator. However, while the magnetization $\langle \mathbf{S} \rangle$ is bounded inside the Bloch sphere in the disentanglement–based model (for any finite number of
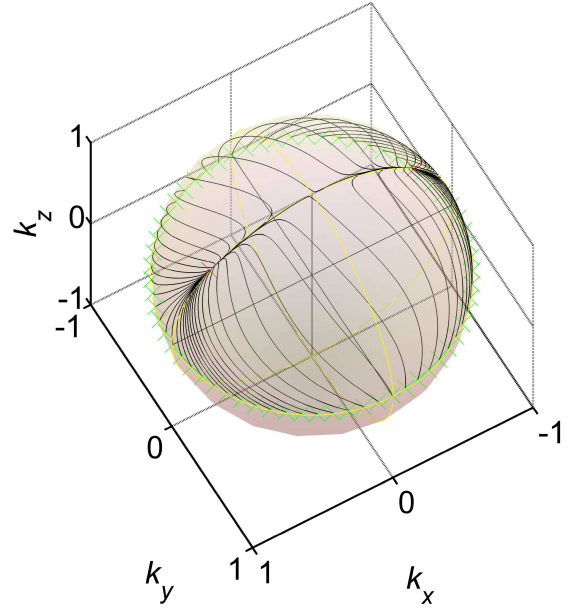

FIG. 1: Two spins. Time evolution of the magnetization $\langle \mathbf{S} \rangle = (k_x, k_y, k_z)$ for the case $L = 2$. Initial states along the Bloch sphere equator are labelled by green $\times$ symbols, and the two locally–stable steady states by red $\times$ symbols. Assumed parameters' values are $\omega_{\mathrm{K}} = 0$, $\Omega_{\mathrm{T}1} = 0$, $\omega_{\mathrm{d}} = 0$, $\gamma_{\mathrm{D}}/\omega_{\mathrm{A}} = 100$, $\Omega_{\mathrm{L}1}/\omega_{\mathrm{A}} = 3/2$ and $\omega_{\mathrm{A}} T_1 = \omega_{\mathrm{A}} T_2 = 0.2$.

spins L), the amplitude of a classical resonator is unbounded.

Rapid disentanglement limit – The demonstration shown in Fig. 1 for disentanglement–induced bistability of a two–spin system (i.e. $L = 2$) is performed by numerically integrating the master equation (1). This method becomes intractable unless L is kept sufficiently small. On the other hand, the rapid disentanglement approximation, which is based on the assumption that the rate of disentanglement γ_{D} is much larger than all decay rates, can significantly simplify the dynamics.

A theoretical model based on the rapid disentanglement approximation [12] is derived in SM section S3. It is found that in this approximation, the expectation value $P_z = \langle S_z \rangle$ satisfies in steady state a cubic polynomial equation given by [see Eq. (S29) in SM section S3]

$$
\frac{P_z}{P_{z0}} = \frac{1}{1 + \dfrac{2W}{\alpha + \left(\delta - 4\sqrt{D}\frac{P_z}{P_{z0}}\right)^2}} , \tag{3}
$$

where P_{z0} represents the steady state value of P_z for the case where $\Omega_{\mathrm{T}1} = 0$ and $\Omega_{\mathrm{L}1} = 0$ (no driving), W is a phase–dependent dimensionless driving amplitude, δ is a dimensionless detuning, and $\sqrt{D}$ is a dimensionless transverse lifetime. To first order in the ratio $\omega_{\mathrm{A}}/\omega_{\mathrm{K}}$, the dimensionless parameters W, δ and D are given by $W = (1/2)|\Omega_{\mathrm{T}1}|^2 T_1 T_2 \left[1 + \sqrt{1-\alpha} \sin\left(2\phi_{\mathrm{T}}\right)\right]$, $\delta = \left(\omega_{\mathrm{T}} - \omega_0\right) T_2$ and $\sqrt{D} = \omega_{\mathrm{K}} T_2 P_{z0}/4$, and to low-

est nonvanishing order in ω_A/ω_K, α is given by $\alpha = 1 - \left((1/2)\left(\omega_A/\omega_K\right)\Omega_{L1}T_2\right)^2$.

Bistability occurs in the region where the cubic polynomial equation (3) has three real solutions (two of which representing locally stable steady states). For the case $\alpha \geq D$ bistability is excluded. For $0 < \alpha < D$, bistability is possible for dimensionless driving amplitudes W bounded by $W \in (W_-, W_+)$ (see Fig. S1 in SM section S3). Analytical expressions for the lower W_- and upper W_+ bounds are derived in SM section S3.

Experimental setup – A FMSR is employed for experimentally testing predictions derived from the spontaneous disentanglement hypothesis. This magnetically–tunable spin system [19] has a variety of applications in many fields, including magnonics [8, 20–26] and quantum data processing [27–31].

A sketch of the experimental setup is shown in Fig. 2(a). The FMSR, which has a radius of $R_s = 125\,\mu m$, is made of Calcium Vanadium Bismuth Iron Garnet (CVBIG, $Ca_2VBiFe_4O_{12}$). The angular frequency of the FMSR Kittel (uniform) mode ω_0 is approximately given by $\omega_0 = \mu_0\gamma_e H_s$ [32], where $\mathbf{H}_s$ is the static magnetic field, $H_s = |\mathbf{H}_s|$, μ_0 is the free space permeability, and $\gamma_e/2\pi = 28\,GHz\,T^{-1}$ is the gyromagnetic ratio [33]. The static magnetic field $\mathbf{H}_s$ is applied using an electromagnet. In comparison with Yttrium-Iron-Garnet [34], which is more commonly used, the smallest value of H_s, for which the FMSR becomes fully magnetized, is significantly lower in CVBIG [35]. To allow lowering $\omega_0/\left(2\pi\right)$ well below $3\,GHz$, CVBIG was chosen for the current study. FMSR reflectivity is measured using a vector network analyzer (VNA), and FMSR response is monitored using a radio frequency spectrum analyzer (RFSA).

The plots shown in Fig. 2(b-f) demonstrate some of the well–known nonlinear effects that are observable with FMSRs [5]. Driving–induced resonance line shape distortion is demonstrated by the plots in Fig. 2 (b) and (c), which exhibit measurements of TLA reflectivity R_{TLA}. The dependency of resonance line shape on longitudinal P_L and transverse P_T driving powers, that are applied to the LLA and TLA, is shown in Fig. 2(b) and (c), respectively. The plots in Fig. 2 (b) and (c) demonstrate that the FMSR response to externally–applied driving is qualitatively similar to the response of classical Mathieu and Duffing oscillators [2].

Frequency mixing between simultaneously applied transverse and longitudinal driving is demonstrated in two different configurations. In the first configuration [see Fig. 2(d)], the longitudinal driving angular frequency, which is denoted by ω_L, is tuned close to $2\omega_T$, whereas $\omega_L \ll \omega_T$ for the second configuration [see Fig. 2 (e) and (f)]. For practical applications, the first configuration is mainly used for phase–sensitive amplification, whereas signal modulation can be implemented using the second configuration [19].

For the first configuration, for which $\omega_L = 2\left(\omega_T + \omega_f\right)$, the effect of the relative phase ϕ_T between the transverse and longitudinal driving tones [see Eq. (2)], is demon-

strated using an intermodulation measurement [36]. The color coded plot in Fig. 2(d) displays the spectral peak intensity (measured using the RFSA) of the first order frequency mixing between transverse and longitudinal driving tones, which occurs at angular frequency $\omega_L - \omega_T = \omega_T + 2\omega_f$. For the second configuration, the longitudinal driving frequency $\omega_L/\left(2\pi\right)$ is tuned to the value $0.5\,MHz$. The measured RFSA trace shown in Fig. 2 (e) contains a sequence of sidebands at angular frequencies $\omega_T + m\omega_L$, where m is an integer. For comparison, a calculated spectral density, which is based on Eq. (D11) of Ref. [37] (see also Ref. [38]), is shown in Fig. 2 (f). Parameters' values are listed in the caption of Fig. 2.

A quantitative comparison between data and predictions derived from the disentanglement–based model is demonstrated by the plots shown in Fig. 3. The effect of driving on resonance line shape can be characterized by the frequency shift of the peak (i.e. extremum) point, which is denoted by f_{dPP}. For the rapid disentanglement model, f_{dPP} can be obtained from Eq. (S31) of SM section S3. A comparison between data and values derived from Eq. (S31) is shown in Fig. 3. Dependency on P_T (transverse driving power) and P_L (longitudinal driving power) is shown in (a) and (b), respectively. Parameters' assumed values are listed in the caption of Fig. 3. The data–theory comparison demonstrates that the disentanglement–based model is capable of qualitatively accounting for the experimentally observed nonlinear response of the spin system under study.

Bosonization – While the linearity of standard QM excludes multistability in finite quantum systems, some approximation methods can give rise to nonlinear dynamics. The method of Bosonization introduces nonlinearity that can give rise to bistability in the presence of magnetic anisotropy [8, 12]. However, it has remained unclear how this method, which yields bistability that is otherwise excluded, can be justified [12].

The application of the Bosonization method to the under–study system of parametrically driven spins is reviewed in SM section S4. For simplicity, it is assumed that FMSR magnetization is uniform (the validity of this assumption is discussed in SM section S4). FMSR damping is characterized by linear $\gamma = \gamma_1 + \gamma_2$ and nonlinear γ_3 rates, where γ_1 and γ_2 represent, respectively, the FMSR–TLA inductive coupling, and intrinsic FMSR loss. Transverse driving is characterized by an amplitude ω_{T1}, relative phase ϕ_T, and angular detuning frequency Ω_d.

The Bosonization method yields in steady state a cubic polynomial equation for the magnon number expectation value E, which is given by [see Eq. (S51) in SM section S4]

$$E = \frac{2\gamma_1\Omega_1}{\left(\Omega_d - \omega_K E\right)^2 + \left(\gamma + \gamma_3 E\right)^2}\,, \tag{4}$$

where $\Omega_1 = \omega_{T1}g_M$. The term g_M represents parametric gain, which periodically depends on the relative phase ϕ_T [see Eq. (S51) of SM section S4]. Note that a relation
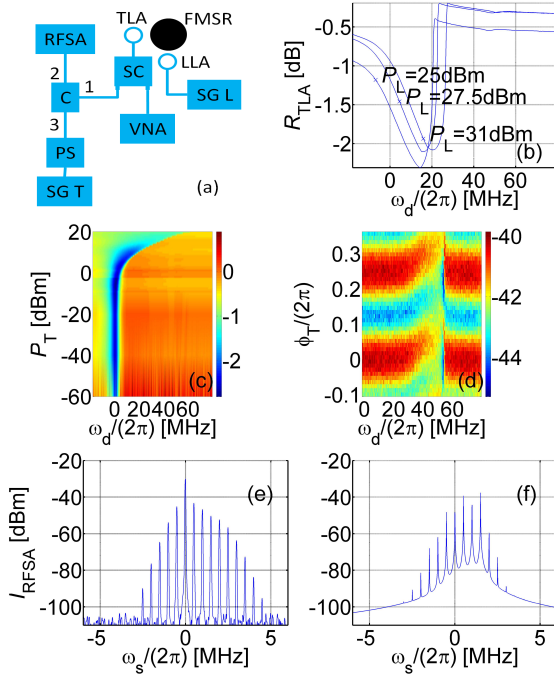
FIG. 2: FMSR. (a) Experimental setup. The FMSR is inductively coupled to two loop antennas (LA), which allow both driving and detection of FMSR magnetic resonance. The signal generators labeled as SG L and SG T drive the longitudinal and transverse loop antennas (LLA and TLA), respectively. A tunable phase shifter (PS) controls the relative phase ϕ_T between longitudinal and transverse driving tones [see Eq. (2)]. A circulator (C) and a splitter/combiner (SC) are used to direct the input and output microwave signals. The LLA (TLA) axis is parallel (perpendicular) to the applied static magnetic field $\mathbf{H}_s$. All measurements are performed at room temperature. The transverse driving frequency $\omega_T/(2\pi)$ is set to 1.874 GHz, and the resonance frequency $\omega_0/(2\pi)$ is tuned by adjusting the electromagnet current. (b) TLA reflectivity R_{TLA} as a function of transverse driving detuning frequency $\omega_d/(2\pi) = (\omega_T - \omega_0)/(2\pi)$ for 3 different values of the driving power applied to the LLA, which is denoted by P_L. The transverse driving power, which is denoted by P_T, is 10 dBm. (c) TLA reflectivity R_{TLA} (in dB units) as a function of transverse driving detuning frequency $\omega_d/(2\pi)$ and P_T (for this measurement no longitudinal driving is applied). (d) Intermodulation peak intensity (in dBm units) as a function of transverse driving detuning frequency $\omega_d/(2\pi)$ and relative phase ϕ_T (controlled by the PS). The longitudinal driving detuning frequency $\omega_f/(2\pi)$ is set to 5 kHz. The intermodulation peak at frequency $(\omega_T + 2\omega_f)/(2\pi)$ is measured using the RFSA. For this measurement $P_T = 10$ dBm and $P_L = 30$ dBm. (e) Mixing with low–frequency longitudinal driving. The measured RFSA intensity I_{RFSA} is plotted as a function of $\omega_s \equiv \omega_{RFSA} - \omega_T$, where ω_{RFSA} is the RFSA angular frequency. Longitudinal driving frequency is $\omega_L/(2\pi) = 0.5$ MHz, and power is 0 dBm. (f) Theoretical calculation of I_{RFSA} based on Eq. (D11) of Ref. [37]. FMSR measured parameters that are used for the calculation are $\omega_L T_1 = 0.6$ and $T_1/T_2 = 2.1$.
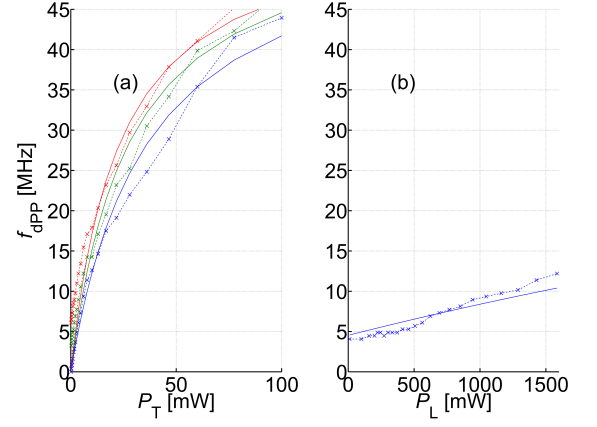

FIG. 3: Peak points. (a) The peak point frequency shift f_{dPP} as a function of transverse driving power P_T for longitudinal driving power P_L values of 0 mW (blue), 320 mW (green) and 560 mW (red). (b) The dependency on longitudinal driving power P_L, for the case $P_T = 31.6$ mW. For both plots, solid lines represent predictions derived using Eq. (S31) of SM section S3. The dimensionless parameter D in Eq. (S31) is determined by measuring the transverse driving power and frequency detuning at the lower bistability onset point (see SM section S3). A calibration yields the dimensionless parameters $W = P_T/(37\,\mathrm{mW})$ and $W_A^2 T_2^2 = P_L/(980\,\mathrm{mW})$.

similar to Eq. (4) is obtained from the Mathieu model for the steady state of a parametrically driven classical resonator [39].

Stability analysis of the cubic polynomial equation (4) has been performed in Ref. [40]. Bistability occurs provided that $|\omega_K| \geq \sqrt{3}\gamma_3$. In the bistability region the cubic polynomial equation (4) has three real non–negative solutions (two of which represent locally stable steady states). For $|\omega_K| \geq \sqrt{3}\gamma_3$, bistability is possible for driving amplitudes Ω_1 bounded by $\Omega_1 \geq \Omega_{1c}$, where $\Omega_{1c} = E_c^3\left(\omega_K^2 + \gamma_3^2\right)/(2\gamma_1)$ and $E_c = \left(2\gamma/\sqrt{3}\right)/\left(|\omega_K| - \sqrt{3}\gamma_3\right)$.

Above parametric instability threshold, and in the absence of nonlinear damping (i.e. for $\gamma_3 = 0$), the Bosonization–based model predicts that the Bosonic mode amplitude exponentially increases as a function of time. A finite steady state solution is obtained provided that $\gamma_3 > 0$. Nonlinear damping in magnetically ordered dielectrics has been theoretically studied in [41]. A pairing mechanism, which originates from a fourth order interaction, suppresses pumping–induced magnon creation [5], and thus further bounds steady state amplitude.

The two competing theoretical models yield distinguishable predictions. For example, the region where bistability occurs in the plane of driving amplitude and driving frequency detuning is finite according to the rapid disentanglement model (see Fig. S1 in SM section S3). In contrast, the Bosonization–based model predicts an infinite region (both driving amplitude Ω_1 and detuning angular frequency Ω_d in the bistability region do not have

upper bounds, see Fig. S2 in SM section S4).

Mapping measurements of the region of bistability are presented in SM section S5. A comparison between data and theoretical predictions (see Fig. S3 of SM section S5) reveals that the rapid disentanglement model better aligns with data (in comparison with the Bosonization–based model).

Discussion – The experimentally–observed effect of parallel pumping on spins suggests that the underlying dynamics are nonlinear [5]. The method of Bosonization can give rise to nonlinearity. However, the justification of this method is arguably questionable [42–46], since it gives rise to multi-stability that is otherwise theoretically excluded. An alternative model, which is based on the disentanglement master equation (1), is found to be capable of qualitatively accounting for both instability and bistability, which are experimentally–observed in the spin system under study.

Generally, the modified master equation (1) can be constructed for any physical system whose Hilbert space has finite dimensionality. The nonlinear term added to the master equation (1) does not violate both norm conservation and positivity of the density operator ρ [10]. For a multipartite system, partial disentanglement (i.e. disentanglement between any pair of subsystems) can be introduced. In the absence of entanglement (i.e. for product states), the nonlinear extension in the master equation (1) does not vary any prediction of standard QM. Disentanglement is invariant under any subsystem unitary transformation, and it is applicable for both distinguishable and indistinguishable particles [47]. Moreover, the spontaneous disentanglement hypothesis is falsifiable, since Eq. (1) yields predictions that are distinguishable from what is derived from standard QM.

The spontaneous disentanglement hypothesis is arguably relevant to the problem of quantum measurement [48–57], which was first introduced in 1935 by Schrödinger [58]. This problem was the main motivation for previously–proposed nonlinear extensions to QM [59–67]. The nonlinear extension in the disentanglement master equation (1) makes the collapse postulate of QM redundant. Moreover, the spontaneous disentanglement hypothesis is arguably related to phase transitions in quantum systems [10] and to superconductivity [47].

Summary – The current study compares predictions derived from two competing theoretical models, with the measured FMSR response to externally–applied transverse and longitudinal driving. Better agreement is obtained from the disentanglement–based model (in comparison with the Bosonization–based model). Further study is needed to determine whether the spontaneous disentanglement hypothesis is consistent with experimental observations obtained with other physical systems, and whether it is internally consistent.

[1] Émile Mathieu, "Mémoire sur le mouvement vibratoire d'une membrane de forme elliptique", *Journal de mathématiques pures et appliquées*, vol. 13, pp. 137–203, 1868.

[2] L. D. Landau and E. M. Lifshitz, *Mechanics, Volume 1 of Course of Theoretical Physics*, Pergamon Press, 1960.

[3] Tomosato Hioki and Eiji Saitoh, "Stochastic dynamics of a metal magnon parametron", *Journal of Applied Physics*, vol. 132, no. 20, pp. 203901, 2022.

[4] M Wanic, Z Toklikishvili, SK Mishra, M Trybus, and L Chotorlishvili, "Magnetoelectric fractals, magnetoelectric parametric resonance and hopf bifurcation", *Physica D: Nonlinear Phenomena*, vol. 467, pp. 134257, 2024.

[5] VS Lvov and LA Prozorova, "Spin waves above the threshold of parametric excitations", *Spin waves and magnetic excitations*, vol. 239, pp. 233, 1988.

[6] N Bloembergen and RW Damon, "Relaxation effects in ferromagnetic resonance", *Physical Review*, vol. 85, no. 4, pp. 699, 1952.

[7] T Holstein and Hl Primakoff, "Field dependence of the intrinsic domain magnetization of a ferromagnet", *Physical Review*, vol. 58, no. 12, pp. 1098, 1940.

[8] Yi-Pu Wang, Guo-Qiang Zhang, Dengke Zhang, Xiao-Qing Luo, Wei Xiong, Shuai-Peng Wang, Tie-Fu Li, C-M Hu, and JQ You, "Magnon kerr effect in a strongly coupled cavity-magnon system", *Physical Review B*, vol. 94, no. 22, pp. 224410, 2016.

[9] Davide Nigro, "On the uniqueness of the steady-state solution of the lindblad–gorini–kossakowski–sudarshan equation", *Journal of Statistical Mechanics: Theory and Experiment*, vol. 2019, no. 4, pp. 043202, 2019.

[10] Eyal Buks, "Disentanglement-induced multistability", *Physical Review A*, vol. 110, no. 1, pp. 012439, 2024.

[11] Eyal Buks, "Spontaneous disentanglement and thermalization", *Advanced Quantum Technologies*, p. 2400036, 2024.

[12] Eyal Buks, "Disentanglement–induced bistability in a magnetic resonator", *Advanced Quantum Technologies*, p. 2400587, 2025.

[13] R Grimaudo, Asm De Castro, M Kuś, and A Messina, "Exactly solvable time-dependent pseudo-hermitian su (1, 1) hamiltonian models", *Physical Review A*, vol. 98, no. 3, pp. 033835, 2018.

[14] K Kowalski and J Rembieliński, "Integrable nonlinear evolution of the qubit", *Annals of Physics*, vol. 411, pp. 167955, 2019.

[15] Andreas Elben, Richard Kueng, Hsin-Yuan Robert Huang, Rick van Bijnen, Christian Kokail, Marcello Dalmonte, Pasquale Calabrese, Barbara Kraus, John Preskill, Peter Zoller, et al., "Mixed-state entanglement from local randomized measurements", *Physical Review Letters*, vol. 125, no. 20, pp. 200501, 2020.

[16] Gian Paolo Beretta, "Nonlinear model dynamics for closed-system, constrained, maximal-entropy-generation relaxation by energy redistribution", *Physical Review E*, vol. 73, no. 2, pp. 026113, 2006.

[17] Goran Lindblad, "On the generators of quantum dynamical semigroups", *Communications in Mathematical*

Physics, vol. 48, no. 2, pp. 119–130, 1976.

[18] Eyal Buks, *Quantum mechanics - Lecture Notes*, http://buks.net.technion.ac.il/teaching/, 2025.

[19] Daniel D Stancil and Anil Prabhakar, *Spin waves*, Springer, 2009.

[20] H Suhl, "The theory of ferromagnetic resonance at high signal powers", *Journal of Physics and Chemistry of Solids*, vol. 1, no. 4, pp. 209–227, 1957.

[21] Shasha Zheng, Zhenyu Wang, Yipu Wang, Fengxiao Sun, Qiongyi He, Peng Yan, and HY Yuan, "Tutorial: nonlinear magnonics", *Journal of Applied Physics*, vol. 134, no. 15, pp. 151101, 2023.

[22] Babak Zare Rameshti, Silvia Viola Kusminskiy, James A Haigh, Koji Usami, Dany Lachance-Quirion, Yasunobu Nakamura, Can-Ming Hu, Hong X Tang, Gerrit EW Bauer, and Yaroslav M Blanter, "Cavity magnonics", *Physics Reports*, vol. 979, pp. 1–61, 2022.

[23] Silvia Viola Kusminskiy, "Cavity optomagnonics", in *Optomagnonic Structures: Novel Architectures for Simultaneous Control of Light and Spin Waves*, pp. 299–353. World Scientific, 2021.

[24] Yi-Pu Wang, Guo-Qiang Zhang, Dengke Zhang, Tie-Fu Li, C-M Hu, and JQ You, "Bistability of cavity magnon polaritons", *Physical review letters*, vol. 120, no. 5, pp. 057202, 2018.

[25] P Hyde, BM Yao, YS Gui, Guo-Qiang Zhang, JQ You, and C-M Hu, "Direct measurement of foldover in cavity magnon-polariton systems", *Physical Review B*, vol. 98, no. 17, pp. 174423, 2018.

[26] Dominik M Juraschek, Derek S Wang, and Prineha Narang, "Sum-frequency excitation of coherent magnons", *Physical Review B*, vol. 103, no. 9, pp. 094407, 2021.

[27] Dany Lachance-Quirion, Yutaka Tabuchi, Arnaud Gloppe, Koji Usami, and Yasunobu Nakamura, "Hybrid quantum systems based on magnonics", *Applied Physics Express*, vol. 12, no. 7, pp. 070101, 2019.

[28] Dany Lachance-Quirion, Samuel Piotr Wolski, Yutaka Tabuchi, Shingo Kono, Koji Usami, and Yasunobu Nakamura, "Entanglement-based single-shot detection of a single magnon with a superconducting qubit", *arXiv:1910.09096*, 2019.

[29] Yutaka Tabuchi, Seiichiro Ishino, Atsushi Noguchi, Toyofumi Ishikawa, Rekishu Yamazaki, Koji Usami, and Yasunobu Nakamura, "Quantum magnonics: The magnon meets the superconducting qubit", *Comptes Rendus Physique*, vol. 17, no. 7, pp. 729–739, 2016.

[30] Mehrdad Elyasi, Yaroslav M Blanter, and Gerrit EW Bauer, "Resources of nonlinear cavity magnonics for quantum information", *Physical Review B*, vol. 101, no. 5, pp. 054402, 2020.

[31] Zhedong Zhang, Marlan O Scully, and Girish S Agarwal, "Quantum entanglement between two magnon modes via kerr nonlinearity driven far from equilibrium", *Physical Review Research*, vol. 1, no. 2, pp. 023021, 2019.

[32] Laurence R Walker, "Magnetostatic modes in ferromagnetic resonance", *Physical Review*, vol. 105, no. 2, pp. 390, 1957.

[33] PC Fletcher and RO Bell, "Ferrimagnetic resonance modes in spheres", *Journal of Applied Physics*, vol. 30, no. 5, pp. 687–698, 1959.

[34] AA Serga, AV Chumak, and B Hillebrands, "Yig magnonics", *Journal of Physics D: Applied Physics*, vol. 43, no. 26, pp. 264002, 2010.

[35] RT Lynch Jr, JF Dillon Jr, and LG Van Uitert, "Stress birefringence in ferrimagnetic garnets", *Journal of Applied Physics*, vol. 44, no. 1, pp. 225–229, 1973.

[36] Cijy Mathai, Sergei Masis, Oleg Shtempluck, Shay Hacohen-Gourgy, and Eyal Buks, "Frequency mixing in a ferrimagnetic sphere resonator", *Euro. Phys. Lett.*, vol. 131, 2020.

[37] Eyal Buks, Chunqing Deng, Jean-Luc F. X. Orgazzi, Martin Otto, and Adrian Lupascu, "Superharmonic resonances in a strongly coupled cavity-atom system", *Phys. Rev. A*, vol. 94, pp. 033807, Sep 2016.

[38] SN Shevchenko, S. Ashhab, and F. Nori, "Landau–zener–stückelberg interferometry", *Physics Reports*, vol. 492, no. 1, pp. 1–30, 2010.

[39] Ron Lifshitz and Michael C Cross, "Nonlinear dynamics of nanomechanical and micromechanical resonators", *Reviews of nonlinear dynamics and complexity*, vol. 1, no. 1, 2008.

[40] Bernard Yurke and Eyal Buks, "Performance of cavity-parametric amplifiers, employing kerr nonlinearites, in the presence of two-photon loss", *J. Lightwave Tech.*, vol. 24, pp. 5054–5066, 2006.

[41] Victor Lvov and GE FALKOVICH, "Interaction between parametrically excited spin-waves and thermal spin-waves", *Zhurnal Eksperimentalnoi I Teoreticheskoi Fiziki*, vol. 82, no. 5, pp. 1562–1577, 1982.

[42] Itamar Katz, Alex Retzker, Raphael Straub, and Ron Lifshitz, "Signatures for a classical to quantum transition of a driven nonlinear nanomechanical resonator", *Physical review letters*, vol. 99, no. 4, pp. 040404, 2007.

[43] Nikita Leppenen and Ephraim Shahmoon, "Quantum bistability at the interplay between collective and individual decay", *arXiv:2404.02134*, 2024.

[44] Fabrizio Minganti, Alberto Biella, Nicola Bartolo, and Cristiano Ciuti, "Spectral theory of liouvillians for dissipative phase transitions", *Physical Review A*, vol. 98, no. 4, pp. 042118, 2018.

[45] Filippo Vicentini, Fabrizio Minganti, Riccardo Rota, Giuliano Orso, and Cristiano Ciuti, "Critical slowing down in driven-dissipative bose-hubbard lattices", *Physical Review A*, vol. 97, no. 1, pp. 013853, 2018.

[46] Haggai Landa, Marco Schiró, and Grégoire Misguich, "Multistability of driven-dissipative quantum spins", *Physical Review Letters*, vol. 124, no. 4, pp. 043601, 2020.

[47] Eyal Buks, "Disentanglement–induced superconductivity", *Entropy*, vol. 27, no. 6, pp. 630, 2025.

[48] Roger Penrose, "Uncertainty in quantum mechanics: faith or fantasy?", *Philosophical Transactions of the Royal Society A: Mathematical, Physical and Engineering Sciences*, vol. 369, no. 1956, pp. 4864–4890, 2011.

[49] Angelo Bassi, Kinjalk Lochan, Seema Satin, Tejinder P Singh, and Hendrik Ulbricht, "Models of wave-function collapse, underlying theories, and experimental tests", *Reviews of Modern Physics*, vol. 85, no. 2, pp. 471, 2013.

[50] Philip Pearle, "Reduction of the state vector by a nonlinear schrödinger equation", *Physical Review D*, vol. 13, no. 4, pp. 857, 1976.

[51] Gian Carlo Ghirardi, Alberto Rimini, and Tullio Weber, "Unified dynamics for microscopic and macroscopic systems", *Physical review D*, vol. 34, no. 2, pp. 470, 1986.

[52] Angelo Bassi and GianCarlo Ghirardi, "Dynamical reduction models", *Physics Reports*, vol. 379, no. 5-6, pp. 257–426, 2003.

[53] Charles H Bennett, Debbie Leung, Graeme Smith, and John A Smolin, "Can closed timelike curves or nonlin-

ear quantum mechanics improve quantum state discrimination or help solve hard problems?", *Physical review letters*, vol. 103, no. 17, pp. 170502, 2009.

[54] Krzysztof Kowalski, "Linear and integrable nonlinear evolution of the qutrit", *Quantum Information Processing*, vol. 19, no. 5, pp. 1–31, 2020.

[55] Bernd Fernengel and Barbara Drossel, "Bifurcations and chaos in nonlinear lindblad equations", *Journal of Physics A: Mathematical and Theoretical*, vol. 53, no. 38, pp. 385701, 2020.

[56] Jonathan Oppenheim, "A postquantum theory of classical gravity?", *Physical Review X*, vol. 13, no. 4, pp. 041040, 2023.

[57] Björn Schrinski, Yu Yang, Uwe von Lüpke, Marius Bild, Yiwen Chu, Klaus Hornberger, Stefan Nimmrichter, and Matteo Fadel, "Macroscopic quantum test with bulk acoustic wave resonators", *Physical Review Letters*, vol. 130, no. 13, pp. 133604, 2023.

[58] E. Schrodinger, "Die gegenwartige situation in der quantenmechanik", *Naturwissenschaften*, vol. 23, pp. 807, 1935.

[59] Steven Weinberg, "Precision tests of quantum mechanics", in *THE OSKAR KLEIN MEMORIAL LECTURES 1988–1999*, pp. 61–68. World Scientific, 2014.

[60] H-D Doebner and Gerald A Goldin, "Introducing nonlinear gauge transformations in a family of nonlinear schrödinger equations", *Physical Review A*, vol. 54, no. 5, pp. 3764, 1996.

[61] Nicolas Gisin and Ian C Percival, "The quantum-state diffusion model applied to open systems", *Journal of Physics A: Mathematical and General*, vol. 25, no. 21, pp. 5677, 1992.

[62] Nicolas Gisin, "A simple nonlinear dissipative quantum evolution equation", *Journal of Physics A: Mathematical and General*, vol. 14, no. 9, pp. 2259, 1981.

[63] Nicolas Gisin, "Weinberg's non-linear quantum mechanics and supraluminal communications", *Physics Letters A*, vol. 143, no. 1-2, pp. 1–2, 1990.

[64] David E Kaplan and Surjeet Rajendran, "Causal framework for nonlinear quantum mechanics", *Physical Review D*, vol. 105, no. 5, pp. 055002, 2022.

[65] Manuel H Muñoz-Arias, Pablo M Poggi, Poul S Jessen, and Ivan H Deutsch, "Simulating nonlinear dynamics of collective spins via quantum measurement and feedback", *Physical review letters*, vol. 124, no. 11, pp. 110503, 2020.

[66] Kurt Jacobs and Daniel A Steck, "A straightforward introduction to continuous quantum measurement", *Contemporary Physics*, vol. 47, no. 5, pp. 279–303, 2006.

[67] Michael R Geller, "Fast quantum state discrimination with nonlinear positive trace-preserving channels", *Advanced Quantum Technologies*, p. 2200156, 2023.

[68] Sergio M Rezende and Flavio M de Aguiar, "Spin-wave instabilities, auto-oscillations, and chaos in yttrium-iron-garnet", *Proceedings of the IEEE*, vol. 78, no. 6, pp. 893–908, 1990.

Supplementary materials: Parametric excitation of a ferrimagnetic sphere resonator

Eyal Buks

Andrew and Erna Viterbi Department of Electrical Engineering, Technion, Haifa 32000 Israel

Heisenberg equations of motion are derived in section S1, and the two–spin case $L = 2$ is discussed in section S2. Sections S3 and S4 are devoted to the rapid disentanglement and the Bosonization–based models, respectively. Predictions derived from these two competing theoretical models are compared with experimental results in section S5.

S1.   EQUATIONS OF MOTION

In this section, a unitary transformation into a rotating frame is applied to simplify the equations of motion. The Hamiltonian given by Eq. (2) in the main text yields Heisenberg equations of motion given by

$$
\frac{\mathrm{d}}{\mathrm{d}t} \begin{pmatrix} S_+ \\ S_- \end{pmatrix} = \begin{pmatrix} -i\omega_z & 0 \\ 0 & i\omega_z \end{pmatrix} \begin{pmatrix} S_+ \\ S_- \end{pmatrix}
$$
$$
+ S_z \begin{pmatrix} -\frac{i\omega_K}{2} & -\frac{i\omega_A}{2} \\ \frac{i\omega_A}{2} & \frac{i\omega_K}{2} \end{pmatrix} \begin{pmatrix} S_+ \\ S_- \end{pmatrix} + \begin{pmatrix} -\frac{i\omega_K}{2} & -\frac{i\omega_A}{2} \\ \frac{i\omega_A}{2} & \frac{i\omega_K}{2} \end{pmatrix} \begin{pmatrix} S_+ \\ S_- \end{pmatrix} S_z
$$
$$
+ \begin{pmatrix} -iS_z\Omega_{T1}^* e^{-i\omega_T t} \\ iS_z\Omega_{T1} e^{i\omega_T t} \end{pmatrix} , \tag{S1}
$$

and [note that $[S_+S_- + S_-S_+, S_z] = 0$, since $S_+S_- + S_-S_+ = 2\left(S_x^2 + S_y^2\right)$]

$$
\frac{\mathrm{d}S_z}{\mathrm{d}t} = -i\frac{\omega_A\left(S_+^2 - S_-^2\right)}{2} - i\frac{\left(S_+\Omega_{T1}e^{i\omega_T t} - S_-\Omega_{T1}^* e^{-i\omega_T t}\right)}{2} . \tag{S2}
$$

The transformation

$$
\begin{pmatrix} \mathcal{S}_+ \\ \mathcal{S}_- \end{pmatrix} = \begin{pmatrix} e^{i\omega_T t} & 0 \\ 0 & e^{-i\omega_T t} \end{pmatrix} \begin{pmatrix} X & Y \\ Y & X \end{pmatrix} \begin{pmatrix} S_+ \\ S_- \end{pmatrix} , \tag{S3}
$$

where $X = (1/2)\left(\sqrt{1 + \omega_A/\omega_K} + \sqrt{1 - \omega_A/\omega_K}\right)$ and where $Y = (1/2)\left(\sqrt{1 + \omega_A/\omega_K} - \sqrt{1 - \omega_A/\omega_K}\right)$, yields [note that $X^2 + Y^2 = 1$, $2XY = \omega_A/\omega_K$, and $X^2 - Y^2 = \sqrt{1 - (\omega_A/\omega_K)^2} = 1/\varrho$, where $\varrho = 1/\sqrt{1 - (\omega_A/\omega_K)^2}$]

$$
\frac{\mathrm{d}}{\mathrm{d}t} \begin{pmatrix} \mathcal{S}_+ \\ \mathcal{S}_- \end{pmatrix} = i \begin{pmatrix} \omega_T - \varrho\omega_z & \varrho\omega_z\frac{\omega_A}{\omega_K}e^{2i\omega_T t} \\ -\varrho\omega_z\frac{\omega_A}{\omega_K}e^{-2i\omega_T t} & -\omega_T + \varrho\omega_z \end{pmatrix} \begin{pmatrix} \mathcal{S}_+ \\ \mathcal{S}_- \end{pmatrix}
$$
$$
+ \frac{i\omega_K}{2\varrho} \begin{pmatrix} -\mathcal{S}_+ S_z - S_z\mathcal{S}_+ \\ \mathcal{S}_- S_z + S_z\mathcal{S}_- \end{pmatrix}
$$
$$
+ i \begin{pmatrix} -X\Omega_{T1}^* + Y\Omega_{T1}e^{2i\omega_T t} \\ X\Omega_{T1} - Y\Omega_{T1}^* e^{-2i\omega_T t} \end{pmatrix} S_z , \tag{S4}
$$

and

$$
\frac{\mathrm{d}S_z}{\mathrm{d}t} = \frac{i\varrho\omega_A\left(e^{2i\omega_T t}\mathcal{S}_-^2 - e^{-2i\omega_T t}\mathcal{S}_+^2\right)}{2}
$$
$$
- i\varrho\frac{X\left(\Omega_{T1}\mathcal{S}_+ - \Omega_{T1}^*\mathcal{S}_-\right) + Y\left(\Omega_{T1}^* e^{-2i\omega_T t}\mathcal{S}_+ - \Omega_{T1}e^{2i\omega_T t}\mathcal{S}_-\right)}{2} . \tag{S5}
$$

In the rotating wave approximation (RWA) Eqs. (S4) and (S5) become [recall that $\omega_T = \omega_0 + \omega_d$ and $\omega_z = $

$\omega_0 + \Omega_{\mathrm{L1}} \cos\left(2\left(\omega_{\mathrm{T}} + \omega_{\mathrm{f}}\right) t\right)$, and note that it is assumed that $|\omega_{\mathrm{d}}| \ll \omega_0$ and $|\omega_{\mathrm{f}}| \ll \omega_0$]

$$\frac{\mathrm{d}}{\mathrm{d}t}\begin{pmatrix} \mathcal{S}_+ \\ \mathcal{S}_- \end{pmatrix} = i \begin{pmatrix} W_{\mathrm{d}} & W_{\mathrm{A}} e^{-2i\omega_{\mathrm{f}}t} \\ -W_{\mathrm{A}} e^{2i\omega_{\mathrm{f}}t} & -W_{\mathrm{d}} \end{pmatrix} \begin{pmatrix} \mathcal{S}_+ \\ \mathcal{S}_- \end{pmatrix}$$
$$+ \frac{iW_{\mathrm{K}}}{2} \begin{pmatrix} -\mathcal{S}_+ S_z - S_z \mathcal{S}_+ \\ \mathcal{S}_- S_z + S_z \mathcal{S}_- \end{pmatrix}$$
$$+ i \begin{pmatrix} -W_{\mathrm{T1}}^* S_z \\ W_{\mathrm{T1}} S_z \end{pmatrix},$$

(S6)

and

$$\frac{\mathrm{d}S_z}{\mathrm{d}t} = \frac{i\varrho\left(W_{\mathrm{T1}}^* \mathcal{S}_- - W_{\mathrm{T1}} \mathcal{S}_+\right)}{2}.$$

(S7)

where $W_{\mathrm{d}} = \omega_{\mathrm{T}} - \varrho\omega_0$, $W_{\mathrm{A}} = (\varrho/2)\left(\omega_{\mathrm{A}}/\omega_{\mathrm{K}}\right)\Omega_{\mathrm{L1}}$, $W_{\mathrm{K}} = \omega_{\mathrm{K}}/\varrho$ and $W_{\mathrm{T1}} = \Omega_{\mathrm{T1}}X$. Note that for $\omega_{\mathrm{f}} = 0$ (i.e. vanishing longitudinal driving angular detuning frequency), the equation of motion (S6) becomes time independent.

S2. THE CASE $L = 2$

For sufficiently small number of spins L, some analytical results can be derived. The smallest value, for which disentanglement is relevant, is $L = 2$ (i.e. two spins). For that case, the matrix representation of the Hamiltonian $\mathcal{H}$ [see Eq. (2) in the main text] is given by (recall that $[S_i, S_j] = 2i\epsilon_{ijk}S_k$, $[S_z, S_\pm] = \pm 2S_\pm$ and $[S_+, S_-] = 4S_z$, where $S_\pm = S_x \pm iS_y$)

$$\frac{\mathcal{H}}{\hbar} \doteq \begin{pmatrix} -\omega_z + \omega_{\mathrm{K}} & \omega_{\mathrm{t}} & \omega_{\mathrm{t}} & \omega_{\mathrm{A}} \\ \omega_{\mathrm{t}}^* & \omega_{\mathrm{K}} & \omega_{\mathrm{K}} & \omega_{\mathrm{t}} \\ \omega_{\mathrm{t}}^* & \omega_{\mathrm{K}} & \omega_{\mathrm{K}} & \omega_{\mathrm{t}} \\ \omega_{\mathrm{A}} & \omega_{\mathrm{t}}^* & \omega_{\mathrm{t}}^* & \omega_z + \omega_{\mathrm{K}} \end{pmatrix},$$

(S8)

where $\omega_{\mathrm{t}} = (\Omega_{\mathrm{T1}}/2) e^{i\omega_{\mathrm{T}}t}$. For the case $\omega_{\mathrm{K}} = 0$, $\omega_{\mathrm{t}} = 0$ and $\omega_{\mathrm{T}} = \omega_0$, the non–vanishing entries of the Hamiltonian $\mathcal{H}$ (S8) can be represented by a 2×2 block given by [recall that $\omega_z = \omega_0 + \Omega_{\mathrm{L1}} \cos(2\omega_0 t)$]

$$\frac{\mathcal{H}}{\hbar} \doteq -\omega_0 \begin{pmatrix} 1 & \tan q \\ \tan q & -1 \end{pmatrix} - \Omega_{\mathrm{L1}} \cos(2\omega_0 t) \begin{pmatrix} 1 & 0 \\ 0 & -1 \end{pmatrix},$$

(S9)

where $\tan q = -\omega_{\mathrm{A}}/\omega_0$.

Diagonalization of the static part is performed by the transformation

$$\frac{\mathcal{H}'}{\hbar} = u^{-1}\frac{\mathcal{H}}{\hbar}u \doteq -\frac{\omega_0}{\cos q}\begin{pmatrix} 1 & 0 \\ 0 & -1 \end{pmatrix}$$
$$- \Omega_{\mathrm{L1}} \cos(2\omega_0 t)\begin{pmatrix} \cos q & -\sin q \\ -\sin q & -\cos q \end{pmatrix},$$

(S10)

where

$$u \doteq \begin{pmatrix} \cos\frac{q}{2} & -\sin\frac{q}{2} \\ \sin\frac{q}{2} & \cos\frac{q}{2} \end{pmatrix}.$$

(S11)

A rotating frame transformation yields

$$\frac{\mathcal{H}''}{\hbar} = -iu_0^\dagger \frac{\mathrm{d}u_0}{\mathrm{d}t} + u_0^\dagger \frac{\mathcal{H}'}{\hbar}u_0$$
$$\doteq \omega_0 \frac{\cos q - 1}{\cos q}\begin{pmatrix} 1 & 0 \\ 0 & -1 \end{pmatrix}$$
$$- \Omega_{\mathrm{L1}} \cos(2\omega_0 t)\begin{pmatrix} \cos q & -e^{-2i\omega_0 t}\sin q \\ -e^{2i\omega_0 t}\sin q & -\cos q \end{pmatrix},$$

(S12)

where

$$u_0 \doteq \begin{pmatrix} e^{i\omega_0 t} & 0 \\ 0 & e^{-i\omega_0 t} \end{pmatrix} . \tag{S13}$$

Applying the RWA leads to the Hamiltonian $\mathcal{H}''_{\mathrm{RWA}}$, which has a matrix representation given by

$$\frac{\mathcal{H}''_{\mathrm{RWA}}}{\hbar} \doteq \omega_0 \frac{\cos q - 1}{\cos q} \begin{pmatrix} 1 & 0 \\ 0 & -1 \end{pmatrix} + \frac{\Omega_{\mathrm{L1}} \sin q}{2} \begin{pmatrix} 0 & 1 \\ 1 & 0 \end{pmatrix} . \tag{S14}$$

The transformation inverse to u yields

$$\begin{aligned} \frac{\mathcal{H}'''}{\hbar} &= u \frac{\mathcal{H}''_{\mathrm{RWA}}}{\hbar} u^{-1} \\ &\doteq \omega_0 (\cos q - 1) \begin{pmatrix} 1 & \tan q \\ \tan q & -1 \end{pmatrix} \\ &+ \frac{\Omega_{\mathrm{L1}} \sin q}{2} \begin{pmatrix} -\sin q & \cos q \\ \cos q & \sin q \end{pmatrix} . \end{aligned} \tag{S15}$$

For $\Omega_{\mathrm{L1}} \ll \omega_0$ and $\omega_{\mathrm{A}} \ll \omega_0$, $\mathcal{H}'''$ has a 4×4 matrix representation given by [recall that $q = \tan^{-1}(-\omega_{\mathrm{A}}/\omega_0) = -\omega_{\mathrm{A}}/\omega_0 + O(\omega_{\mathrm{A}}^3)$]

$$\frac{\mathcal{H}'''}{\hbar} \doteq -\frac{\omega_{\mathrm{A}}}{2\omega_0} \begin{pmatrix} \omega_{\mathrm{A}} & 0 & 0 & \Omega_{\mathrm{L1}} \\ 0 & 0 & 0 & 0 \\ 0 & 0 & 0 & 0 \\ \Omega_{\mathrm{L1}} & 0 & 0 & -\omega_{\mathrm{A}} \end{pmatrix} . \tag{S16}$$

S3. RAPID DISENTANGLEMENT APPROXIMATION

The spontaneous disentanglement hypothesis is formulated using a nonlinear master equation given by Eq. (1) in the main text. For large systems, this nonlinear master equation is commonly intractable. In the current section, the rapid disentanglement approximation, which greatly simplifies the dynamics, is explored.

The term $\mathcal{S}_\pm S_z + S_z \mathcal{S}_\pm$ in Eq. (S6) can be expressed as $\mathcal{S}_\pm S_z + S_z \mathcal{S}_\pm = \sum_{l',l''=1}^{L} (\mathcal{S}_{l',\pm} S_{l'',z} + S_{z,l'} \mathcal{S}_{l',\pm})$. The approximation $\langle \mathcal{S}_{l',\pm} S_{l'',z} + S_{z,l'} \mathcal{S}_{l',\pm} \rangle \simeq \langle \mathcal{S}_{l',\pm} \rangle \langle S_{l'',z} \rangle + \langle S_{z,l'} \rangle \langle \mathcal{S}_{l',\pm} \rangle \simeq 2L^{-2} \langle \mathcal{S}_\pm \rangle \langle S_z \rangle$ can be implemented provided that the rate of disentanglement γ_{D} is sufficiently large. By implementing this approximation, and by averaging and adding damping terms to Eqs. (S6) and (S7), one obtains

$$\begin{aligned} &\frac{\mathrm{d}}{\mathrm{d}t} \begin{pmatrix} P_+ \\ P_- \end{pmatrix} \\ &= \begin{pmatrix} i(W_{\mathrm{d}} - W_{\mathrm{K}} P_z) - \frac{1}{T_2} & iW_{\mathrm{A}} e^{-2i\omega_{\mathrm{f}} t} \\ -iW_{\mathrm{A}} e^{2i\omega_{\mathrm{f}} t} & -i(W_{\mathrm{d}} - W_{\mathrm{K}} P_z) - \frac{1}{T_2} \end{pmatrix} \begin{pmatrix} P_+ \\ P_- \end{pmatrix} \\ &+ iP_z \begin{pmatrix} -W_{\mathrm{T1}}^* \\ W_{\mathrm{T1}} \end{pmatrix} , \end{aligned} \tag{S17}$$

and

$$\frac{\mathrm{d}P_z}{\mathrm{d}t} = \frac{i\varrho (W_{\mathrm{T1}}^* P_- - W_{\mathrm{T1}} P_+)}{2} - \frac{P_z - P_{z0}}{T_1} , \tag{S18}$$

where $P_\pm = \langle \mathcal{S}_\pm \rangle$ and $P_z = \langle S_z \rangle$. Note that Eqs. (S17) and (S18) are invariant under the transformation $(\phi_{\mathrm{T}}, P_+, P_-) \to (\phi_{\mathrm{T}} + \pi, -P_+, -P_-)$ (recall that $W_{\mathrm{T1}} = X |\Omega_{\mathrm{T1}}| e^{i\phi_{\mathrm{T}}}$). Note that the same invariance occurs in the classical realm, which is described by the Mathieu model.

For the case $\omega_{\mathrm{f}} = 0$ (no parametric detuning) and $W_{\mathrm{T1}} = 0$ (no transverse driving), Eq. (S17) yields $\mathrm{d}\mathcal{N}/\mathrm{d}t = 2(W_{\mathrm{A}} \sin(2\phi_{\mathrm{P}}) - 1/T_2)\mathcal{N}$, where $\mathcal{N} \equiv P_+ P_- = P_x^2 + P_y^2$, $P_\pm = \sqrt{\mathcal{N}} e^{\pm i\phi_{\mathrm{P}}}$, and ϕ_{P} is real. Phase–dependent rate of magnon creation by parallel pumping is represented by the term $W_{\mathrm{A}} \sin(2\phi_{\mathrm{P}})$ [recall that $W_{\mathrm{A}} = (\varrho/2)(\omega_{\mathrm{A}}/\omega_{\mathrm{K}})\Omega_{\mathrm{L1}}$].

A. The case $\omega_{\rm f} = 0$

For the case $\omega_{\rm f} = 0$ (i.e. no parametric detuning), a unitary transformation given by

$$\begin{pmatrix} P_x \\ P_y \end{pmatrix} = \begin{pmatrix} 1 & i \\ 1 & -i \end{pmatrix}^{-1} \begin{pmatrix} P_+ \\ P_- \end{pmatrix} , \tag{S19}$$

yields real equations of motion given by [see Eqs. (S17) and (S18)]

$$\frac{d\mathbf{P}}{dt} = \begin{pmatrix} -\frac{1}{T_2} & -w_{\rm d} + W_{\rm A} & -W_{\rm T1I} \\ w_{\rm d} + W_{\rm A} & -\frac{1}{T_2} & -W_{\rm T1R} \\ \varrho W_{\rm T1I} & \varrho W_{\rm T1R} & -\frac{1}{T_1} \end{pmatrix} \mathbf{P} + \begin{pmatrix} 0 \\ 0 \\ \frac{P_{z0}}{T_1} \end{pmatrix} , \tag{S20}$$

where $\mathbf{P} = (P_x, P_y, P_z)^{\rm T}$, and where

$$W_{\rm T1R} = \frac{W_{\rm T1} + W_{\rm T1}^*}{2} , \tag{S21}$$

$$W_{\rm T1I} = \frac{W_{\rm T1} - W_{\rm T1}^*}{2i} . \tag{S22}$$

Alternatively

$$\frac{d\mathbf{P}}{dt} = \mathbf{W}_{\rm R} \times \mathbf{P} + M_{\rm d}\mathbf{P} + \begin{pmatrix} 0 \\ 0 \\ \frac{P_{z0}}{T_1} \end{pmatrix} , \tag{S23}$$

where the vector $\mathbf{W}_{\rm R}$, which is given by $\mathbf{W}_{\rm R} = (W_{\rm T1R}, -W_{\rm T1I}, w_{\rm d})^{\rm T}$, represents a rotation axis, and where the matrix $M_{\rm d}$ is given by (note that $W_{\rm A} = 0$ and $\varrho - 1 = 0$ when $\omega_{\rm A} = 0$)

$$M_{\rm d} = \begin{pmatrix} -\frac{1}{T_2} & W_{\rm A} & 0 \\ W_{\rm A} & -\frac{1}{T_2} & 0 \\ (\varrho - 1) W_{\rm T1I} & (\varrho - 1) W_{\rm T1R} & -\frac{1}{T_1} \end{pmatrix} . \tag{S24}$$

The eigenvalues of the matrix $M_{\rm d}$, which represent effective values of spin damping rates, are $-(1 + W_{\rm A}T_2)/T_2$, $-(1 - W_{\rm A}T_2)/T_2$ and $-1/T_1$.

B. Bistability for the case $\omega_{\rm f} = 0$

Steady states, which are time–independent solutions of the equations of motion, are derived in this section. For $\omega_{\rm f} = 0$ (i.e. vanishing longitudinal driving angular detuning frequency), Eq. (S17) can be expressed as

$$\frac{d}{dt} \begin{pmatrix} P_+ \\ P_- \end{pmatrix} = \frac{1}{T_2} M_{\rm T} \begin{pmatrix} P_+ \\ P_- \end{pmatrix} + i z P_{z0} \begin{pmatrix} -W_{\rm T1}^* \\ W_{\rm T1} \end{pmatrix} , \tag{S25}$$

where the matrix $M_{\rm T}$ is given by

$$M_{\rm T} = \begin{pmatrix} i\left(\delta - 4\sqrt{D}z\right) - 1 & i\sqrt{1-\alpha} \\ -i\sqrt{1-\alpha} & -i\left(\delta - 4\sqrt{D}z\right) - 1 \end{pmatrix} , \tag{S26}$$

$\delta = W_{\rm d}T_2$, $D = (W_{\rm K}T_2P_{z0}/4)^2$, $z = P_z/P_{z0}$ and $\alpha = 1 - W_{\rm A}^2T_2^2$. Steady state of Eq. (S25) is given by

$$\begin{pmatrix} P_+ \\ P_- \end{pmatrix} = i z P_{z0} T_2 M_{\rm T}^{-1} \begin{pmatrix} W_{\rm T1}^* \\ -W_{\rm T1} \end{pmatrix} , \tag{S27}$$

and thus (recall that $W_{\rm T1} = |W_{\rm T1}| e^{i\phi_{\rm T}}$)

$$W_{\rm T1}^* P_- - W_{\rm T1} P_+ = 2i z P_{z0} T_2 |W_{\rm T1}|^2 \frac{1 + \sqrt{1-\alpha}\sin(2\phi_{\rm T})}{\alpha + \left(\delta - 4\sqrt{D}z\right)^2} , \tag{S28}$$

hence in steady state [see Eq. (S18)]

$$z = \frac{1}{1 + \frac{2W}{\alpha + (\delta - 4\sqrt{D}z)^2}} \ , \tag{S29}$$

where $W = (1/2)\,\varrho\,|W_{\mathrm{T1}}|^2\,T_1 T_2 \left[1 + \sqrt{1 - \alpha}\sin(2\phi_{\mathrm{T}})\right]$. The cubic polynomial equation for z (S29) can be expressed as $0 = F(z, \delta)$, where

$$F(z, \delta) = z\left(\alpha + \left(\delta - 4\sqrt{D}z\right)^2 + 2W\right) - \alpha - \left(\delta - 4\sqrt{D}z\right)^2 \ . \tag{S30}$$

Peak points – At peak points, for which $0 = \mathrm{d}z/\mathrm{d}\delta = -\left(\partial F/\partial \delta\right)/\left(\partial F/\partial z\right)$, where $\partial F/\partial \delta = 2\left(z - 1\right)\left(\delta - 4\sqrt{D}z\right)$, the condition $0 = F$ yields $z = 1/\left(1 + (2W/\alpha)\right)$ and

$$\delta = \frac{4\sqrt{D}}{1 + \frac{2W}{\alpha}} \ . \tag{S31}$$

Bistability onset points – At a bistability onset point the following three conditions hold

$$0 = \frac{\mathrm{d}\delta}{\mathrm{d}z} = -\frac{F_z}{F_\delta} \ , \tag{S32}$$

$$0 = \frac{\mathrm{d}^2\delta}{\mathrm{d}z^2} = -\frac{F_\delta^2 F_{zz} - 2 F_z F_\delta F_{z\delta} + F_z^2 F_{\delta\delta}}{F_\delta^3} \ , \tag{S33}$$

and

$$0 = F(z, \delta) \ , \tag{S34}$$

where F with an added subscript denotes a partial derivative, e.g. $F_z = \partial F/\partial z$. Solution for z of conditions (S32), (S33) and (S34) are given by $z_1 = Z(q)$, and $z_\pm = Z\left(qe^{\pm 2\pi i/3}\right)$, where the function $Z(x)$ is defined by $Z(x) = (x + 1/x + 3)/4$, and where $q = \exp\left(i\left(2/3\right)\cos^{-1}\sqrt{\alpha/D}\right)$. For any given solution for z, the corresponding variables δ and W are given by $\delta = 2\sqrt{D}(3z - 1)$ and $W = 6D\left(1 - z\right)^2 - \alpha/2$. For the case $1 \leq \alpha/D$ bistability is excluded. For the case $\alpha/D = 1$, the following holds $z_\pm = 1/2$, $\delta = \sqrt{\alpha}$, and $W = \alpha$. For negative α, only a single bistability onset point exists, and for this case bistability occurs only *below* the corresponding critical value of W.

The plot in Fig. S1, which is based on the cubic polynomial equation (S30), displays steady state values of the dimensionless polarization z as a function of the dimensionless detuning δ, for five different values of the dimensionless driving amplitude W. The symbol $P_\pm$ labels the bistability onset point having dimensionless polarization $z_\pm$ and dimensionless detuning $\delta_\pm$. Peak points are labeled by green triangles [see Eq. (S31)].

C. Parametric gain for the case $\omega_{\mathrm{f}} = 0$

The eigenvalues of the matrix M_{T} (S26) are $-1 \pm \sqrt{1 - \alpha - \left(\delta - 4\sqrt{D}z\right)^2}$. This matrix can be decomposed as

$$\begin{aligned}
M_{\mathrm{T}} &= \begin{pmatrix} \mu_1 & \mu_2 \\ \mu_2^* & \mu_1^* \end{pmatrix} \\
&= \begin{pmatrix} |\mu_1|\,e^{i\phi_1} & |\mu_2|\,e^{i\phi_2} \\ |\mu_2|\,e^{-i\phi_2} & |\mu_1|\,e^{-i\phi_1} \end{pmatrix} \\
&= R\left(\frac{\phi_1 + \phi_2}{2}\right)\begin{pmatrix} |\mu_1| + |\mu_2| & 0 \\ 0 & |\mu_1| - |\mu_2| \end{pmatrix} R^\dagger\left(\frac{\phi_2 - \phi_1}{2}\right) \ ,
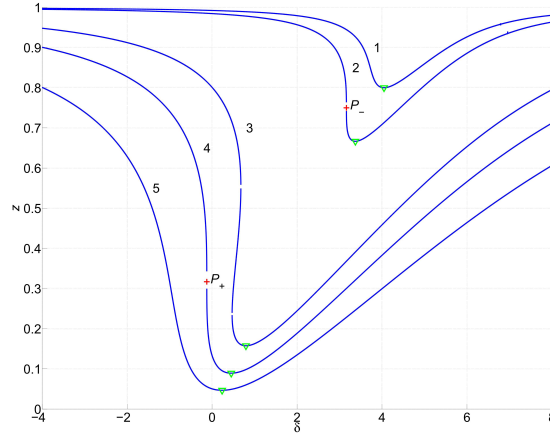\end{aligned} \tag{S35}$$

FIG. S1: Dimensionless polarization z as a function of dimensionless detuning δ for the rapid disentanglement model. Calculation of steady state is based on Eq. (S29). Assumed parameters's values are $\alpha = 0.8$ and $D = 2\alpha$. The five curves, which are labelled by the numbers 1, 2, 3, 4, and 5, are calculated for five different values of the dimensionless driving amplitude W respectively given by $W_-/2$, W_-, $(W_- + W_+)/2$, W_+ and $2W_+$, where $W_\pm$ is the value of W corresponding to the bistability onset point having value of z given by $z_\pm$. Peak points are labeled by green triangles [see Eq. (S31)].

where $\mu_1 = i\left(\delta - 4\sqrt{D}z\right) - 1 = |\mu_1|\, e^{i\phi_1}$, $\mu_2 = i\sqrt{1-\alpha} = |\mu_2|\, e^{i\phi_2}$, and where the unitary matrix $R\left(\phi\right)$ is given by

$$R\left(\phi\right) = \begin{pmatrix} \frac{e^{i\phi}}{\sqrt{2}} & \frac{e^{i\phi}}{\sqrt{2}} \\ \frac{e^{-i\phi}}{\sqrt{2}} & -\frac{e^{-i\phi}}{\sqrt{2}} \end{pmatrix} , \tag{S36}$$

and thus in steady state [see Eq. (S27), recall that $W_{\mathrm{T}1} = |W_{\mathrm{T}1}|\, e^{i\phi_{\mathrm{T}}}$, and note that $|\mu_1|^2 - |\mu_2|^2 = \alpha + \left(\delta - 4\sqrt{D}z\right)^2$]

$$\begin{pmatrix} P_+ \\ P_- \end{pmatrix} = \frac{izP_{z0}T_2\,|W_{\mathrm{T}1}|}{|\mu_1|^2 - |\mu_2|^2}\begin{pmatrix} |\mu_1|\, e^{-i(\phi_{\mathrm{T}}+\phi_1)} + |\mu_2|\, e^{i(\phi_{\mathrm{T}}+\phi_2)} \\ -|\mu_1|\, e^{i(\phi_{\mathrm{T}}+\phi_1)} - |\mu_2|\, e^{-i(\phi_{\mathrm{T}}+\phi_2)} \end{pmatrix} . \tag{S37}$$

The following holds

$$P_+ P_- = \left(\frac{zP_{z0}T_2\,|W_{\mathrm{T}1}|}{|\mu_1|\left(1 - \left|\frac{\mu_2}{\mu_1}\right|^2\right)}\right)^2 g_{\mathrm{P}}\left(\phi_{\mathrm{T}}\right) , \tag{S38}$$

where the phase–dependent gain $g_{\mathrm{P}}\left(\phi_{\mathrm{T}}\right)$ is given by

$$\begin{aligned} g_{\mathrm{P}} &= \left|1 + \frac{|\mu_2|\, e^{2i\left(\phi_{\mathrm{T}}+\frac{\phi_1+\phi_2}{2}\right)}}{|\mu_1|}\right|^2 \\ &= \left(1 + \frac{|\mu_2|}{|\mu_1|}\right)^2 \cos^2\left(\phi_{\mathrm{T}} + \frac{\phi_1+\phi_2}{2}\right) + \left(1 - \frac{|\mu_2|}{|\mu_1|}\right)^2 \sin^2\left(\phi_{\mathrm{T}} + \frac{\phi_1+\phi_2}{2}\right) \\ &= 1 + \frac{2\,|\mu_2|}{|\mu_1|}\cos\left(2\phi_{\mathrm{T}} + \phi_1 + \phi_2\right) + \frac{|\mu_2|^2}{|\mu_1|^2} . \end{aligned} \tag{S39}$$

Note that as a function of ϕ_{T} the gain $g_{\mathrm{P}}\left(\phi_{\mathrm{T}}\right)$ oscillates between a minimum value given by $\left(1 - |\mu_2|\,/\,|\mu_1|\right)^2$ and a maximum value given by $\left(1 + |\mu_2|\,/\,|\mu_1|\right)^2$.

S4. BOSONIZATION

The method of Bosonization is widely employed to study spin systems. As is discussed below, by implementing this method, the equations of motion become nonlinear, and consequently, multistabilities, which are otherwise excluded, become allowed. In the Holstein–Primakoff transformation [S1], the operators $S_\pm$ and S_z are expressed as $S_+ = 2B^\dagger \left(L - B^\dagger B\right)^{1/2}$, $S_- = 2\left(L - B^\dagger B\right)^{1/2} B$ and $S_z = -L + 2B^\dagger B$, where L is the total number of spins, and where $B^\dagger B$ is a number operator. Self–consistency with the originally–assumed commutation relations $[S_+, S_-] = 4S_z$ and $[S_z, S_\pm] = \pm 2S_\pm$ is obtained by requiring that the operators B and $B^\dagger$ satisfy the Bosonic commutation relation $\left[B, B^\dagger\right] = 1$.

The Hamiltonian $\mathcal{H}$ [see Eq. (2) in the main text] can be expressed in terms of the operators B and $B^\dagger$ [S2–S5]. The following holds $(S_+ S_- + S_- S_+)/8 = (L-1) B^\dagger B - B^\dagger B^\dagger B B + L/2$ [see the term proportional to ω_K in the Hamiltonian $\mathcal{H}$ given by Eq. (2) in the main text]. The approximations $S_+ \simeq 2L^{1/2} B^\dagger$ and $S_- \simeq 2L^{1/2} B$, which are based on the assumption that $\left\langle B^\dagger B \right\rangle / L \ll 1$, yield $S_+^2 + S_-^2 = 4L \left(B^\dagger B^\dagger + BB\right)$ [see the term proportional to ω_A in the Hamiltonian $\mathcal{H}$ given by Eq. (2) in the main text].

The terms proportional to Ω_T1 and Ω_T1^* in the Hamiltonian $\mathcal{H}$ given by Eq. (2) in the main text represent transverse driving. In the Bosonization method, these terms are excluded from the closed–system Hamiltonian $\mathcal{H}$, and transverse driving is instead accounted for by introducing an external feedline [S6]. The coupling between the feedline and the spins, which is assumed to be linear, is characterized by a rate denoted by γ_1. Closed–system Heisenberg equations of motion for the operators B and $B^\dagger$ are thus derived by ignoring the transverse driving terms in $\mathcal{H}$ (the approximation $L - 1 \simeq L$ is implemented)

$$
\frac{\mathrm{d}}{\mathrm{d}t} \begin{pmatrix} B^\dagger \\ B \end{pmatrix} = \begin{pmatrix} -i\omega_z + iL\omega_\mathrm{K} & iL\omega_\mathrm{A} \\ -iL\omega_\mathrm{A} & i\omega_z - iL\omega_\mathrm{K} \end{pmatrix} \begin{pmatrix} B^\dagger \\ B \end{pmatrix}
$$
$$
+ 2i\omega_\mathrm{K} \begin{pmatrix} -B^\dagger B^\dagger B \\ B^\dagger B B \end{pmatrix} .
$$

$$(\mathrm{S40})$$

The operator transformation [compare with Eq. (S3), and recall that $X = (1/2)\left(\sqrt{1 + \omega_\mathrm{A}/\omega_\mathrm{K}} + \sqrt{1 - \omega_\mathrm{A}/\omega_\mathrm{K}}\right) = 1 + O\left(\omega_\mathrm{A}^2\right)$ and $Y = (1/2)\left(\sqrt{1 + \omega_\mathrm{A}/\omega_\mathrm{K}} - \sqrt{1 - \omega_\mathrm{A}/\omega_\mathrm{K}}\right) = (1/2)\,\omega_\mathrm{A}/\omega_\mathrm{K} + O\left(\omega_\mathrm{A}^2\right)$]

$$
\begin{pmatrix} \mathcal{B}_+ \\ \mathcal{B}_- \end{pmatrix} = \begin{pmatrix} e^{i\omega_\mathrm{T} t} & 0 \\ 0 & e^{-i\omega_\mathrm{T} t} \end{pmatrix} \begin{pmatrix} X & Y \\ Y & X \end{pmatrix} \begin{pmatrix} B^\dagger \\ B \end{pmatrix} ,
$$

$$(\mathrm{S41})$$

yields [recall that $X^2 + Y^2 = 1$, $2XY = \omega_\mathrm{A}/\omega_\mathrm{K}$, and $X^2 - Y^2 = \sqrt{1 - (\omega_\mathrm{A}/\omega_\mathrm{K})^2} = 1/\varrho$, where $\varrho = 1/\sqrt{1 - (\omega_\mathrm{A}/\omega_\mathrm{K})^2}$]

$$
\frac{\mathrm{d}}{\mathrm{d}t} \begin{pmatrix} \mathcal{B}_+ \\ \mathcal{B}_- \end{pmatrix}
$$
$$
= i \begin{pmatrix} \omega_\mathrm{T} - \varrho\omega_z + \frac{L\omega_\mathrm{K}}{\varrho} & \frac{\varrho\omega_\mathrm{A}\omega_z e^{2i\omega_\mathrm{T} t}}{\omega_\mathrm{K}} \\ -\frac{\varrho\omega_\mathrm{A}\omega_z e^{-2i\omega_\mathrm{T} t}}{\omega_\mathrm{K}} & -\omega_\mathrm{T} + \varrho\omega_z - \frac{L\omega_\mathrm{K}}{\varrho} \end{pmatrix} \begin{pmatrix} \mathcal{B}_+ \\ \mathcal{B}_- \end{pmatrix}
$$
$$
+ 2i\omega_\mathrm{K} \begin{pmatrix} e^{i\omega_\mathrm{T} t} & 0 \\ 0 & e^{-i\omega_\mathrm{T} t} \end{pmatrix} \begin{pmatrix} X & Y \\ Y & X \end{pmatrix} \begin{pmatrix} -B^\dagger B^\dagger B \\ B^\dagger B B \end{pmatrix} .
$$

$$(\mathrm{S42})$$

$$(\mathrm{S43})$$

The transformation inverse to (S41) yields in the RWA (recall that $X^2 + Y^2 = 1$)

$$
\begin{pmatrix} e^{i\omega_\mathrm{T} t} & 0 \\ 0 & e^{-i\omega_\mathrm{T} t} \end{pmatrix} \begin{pmatrix} X & Y \\ Y & X \end{pmatrix} \begin{pmatrix} -B^\dagger B^\dagger B \\ B^\dagger B B \end{pmatrix} = \begin{pmatrix} -\frac{X^2 \mathcal{B}_+ \mathcal{B}_+ \mathcal{B}_- + 2X^2 Y^2 \mathcal{B}_+ \mathcal{B}_- \mathcal{B}_+ + Y^2 \mathcal{B}_- \mathcal{B}_+ \mathcal{B}_+}{(X^2 - Y^2)^3} \\ \frac{X^2 \mathcal{B}_+ \mathcal{B}_- \mathcal{B}_- + 2X^2 Y^2 \mathcal{B}_- \mathcal{B}_+ \mathcal{B}_- + Y^2 \mathcal{B}_- \mathcal{B}_- \mathcal{B}_+}{(X^2 - Y^2)^3} \end{pmatrix} ,
$$

$$(\mathrm{S44})$$

and thus in this approximation [recall that $\omega_z = \omega_0 + \Omega_{L1} \cos\left(2\left(\omega_T + \omega_f\right)t\right)$, and that $W_A = \left(\varrho/2\right)\left(\omega_A/\omega_K\right)\Omega_{L1}$]

$$
\begin{aligned}
&\frac{\mathrm{d}}{\mathrm{d}t}\begin{pmatrix} \mathcal{B}_+ \\ \mathcal{B}_- \end{pmatrix} \\
&= i\begin{pmatrix} \omega_T - \varrho\omega_z + \frac{L\omega_K}{\varrho} & W_A e^{-2i\omega_f t} \\ -W_A e^{2i\omega_f t} & -\omega_T + \varrho\omega_z - \frac{L\omega_K}{\varrho} \end{pmatrix}\begin{pmatrix} \mathcal{B}_+ \\ \mathcal{B}_- \end{pmatrix} \\
&+ 2i\omega_K\begin{pmatrix} -\frac{X^2\mathcal{B}_+\mathcal{B}_+\mathcal{B}_- + 2X^2Y^2\mathcal{B}_+\mathcal{B}_-\mathcal{B}_+ + Y^2\mathcal{B}_-\mathcal{B}_+\mathcal{B}_+}{(X^2-Y^2)^3} \\ \frac{X^2\mathcal{B}_+\mathcal{B}_-\mathcal{B}_- + 2X^2Y^2\mathcal{B}_-\mathcal{B}_+\mathcal{B}_- + Y^2\mathcal{B}_-\mathcal{B}_-\mathcal{B}_+}{(X^2-Y^2)^3} \end{pmatrix} .
\end{aligned}
$$

$$(S45)$$

Damping is characterized by a linear rate given by $\gamma = \gamma_1 + \gamma_2$, and a cubic nonlinear rate denoted by γ_3. The rate γ_2 represents intrinsic FMSR damping (recall that γ_1 characterizes coupling to the feedline). Transverse driving, which is delivered via the external feedline [S7], is characterized by amplitude ω_{T1} (in units of rate) and relative phase ϕ_T.

Equations of motion for the expectation values $\beta_\pm = \langle\mathcal{B}_\pm\rangle$ are obtained by applying averaging to the operator equations of motion (S45), and by adding terms representing damping and transverse driving. In the next step, the mean field approximation is implemented by replacing terms having the form $\langle\mathcal{B}_{\sigma_1}\mathcal{B}_{\sigma_2}\mathcal{B}_{\sigma_3}\rangle$, by $\langle\mathcal{B}_{\sigma_1}\rangle\langle\mathcal{B}_{\sigma_2}\rangle\langle\mathcal{B}_{\sigma_3}\rangle$, where $\sigma_n \in \{+,-\}$ and $n \in \{1,2,3\}$. The validity of the mean field approximation is arguably questionable, because, as can be seen from the derivation below, terms having the form $\langle\mathcal{B}_{\sigma_1}\rangle\langle\mathcal{B}_{\sigma_2}\rangle\langle\mathcal{B}_{\sigma_3}\rangle$ give rise to nonlinear dynamics. Consequently, multistabilities, which are originally excluded, become allowed when the mean field approximation is being implemented. The current manuscript is mainly motivated by the difficulty to justify the mean field approximation.

The equations of motion for the expectation values $\beta_\pm = \langle\mathcal{B}_\pm\rangle$ are (recall that $X^2 + Y^2 = 1$)

$$\frac{\mathrm{d}}{\mathrm{d}t}\begin{pmatrix} \beta_+ \\ \beta_- \end{pmatrix} = M_\beta\begin{pmatrix} \beta_+ \\ \beta_- \end{pmatrix} + \sqrt{2\gamma_1\omega_{T1}}\begin{pmatrix} ie^{-i\phi_T} \\ -ie^{i\phi_T} \end{pmatrix} , \tag{S46}$$

where the 2×2 matrix M_β is given by

$$M_\beta = \begin{pmatrix} W_b & iW_A e^{-2i\omega_f t} \\ -iW_A e^{2i\omega_f t} & W_b^* \end{pmatrix} , \tag{S47}$$

and $W_b = i\left(\omega_T - \varrho\omega_0 + L\omega_K/\varrho - 2\varrho^3\omega_K\left(1 + \left(\omega_A/\omega_K\right)^2/2\right)\beta_+\beta_-\right) - \gamma - \gamma_3\beta_+\beta_-$[compare with Eq. (S35)]. Note that $W_b = i\left(\Omega_d - 2\omega_K\beta_+\beta_-\right) - \gamma - \gamma_3\beta_+\beta_- + O\left(\omega_A^2\right)$, where $\Omega_d = \omega_T - \omega_0 + L\omega_K$.

For the case $\omega_f = 0$, steady state solution of Eq. (S46) is given by

$$
\begin{aligned}
\begin{pmatrix} \beta_+ \\ \beta_- \end{pmatrix} &= -\sqrt{2\gamma_1\omega_{T1}}\begin{pmatrix} \frac{W_b^*}{|W_b|^2 - W_A^2} & -\frac{iW_A}{|W_b|^2 - W_A^2} \\ \frac{iW_A}{|W_b|^2 - W_A^2} & \frac{W_b}{|W_b|^2 - W_A^2} \end{pmatrix}\begin{pmatrix} ie^{-i\phi_T} \\ -ie^{i\phi_T} \end{pmatrix} \\
&= -\frac{\sqrt{2\gamma_1\omega_{T1}}}{|W_b|^2 - W_A^2}\begin{pmatrix} iW_b^* e^{-i\phi_T} - W_A e^{i\phi_T} \\ -W_A e^{-i\phi_T} - iW_b e^{i\phi_T} \end{pmatrix} ,
\end{aligned}
$$

$$(S48)$$

and thus the steady state value of $E \equiv |\beta_\pm|^2 = \beta_+\beta_-$ can be calculated by solving the equation (note that W_b depends on E)

$$E = \frac{2\gamma_1\omega_{T1}g_M}{|W_b|^2\left(1 - \left|\frac{W_A}{W_b}\right|^2\right)^2} , \tag{S49}$$

where the phase–dependent gain $g_M\left(\phi_T\right)$ is given by [compare to Eq. (S39)]

$$g_M = \left|1 + \frac{iW_A e^{2i\phi_T}}{W_b^*}\right|^2 . \tag{S50}$$
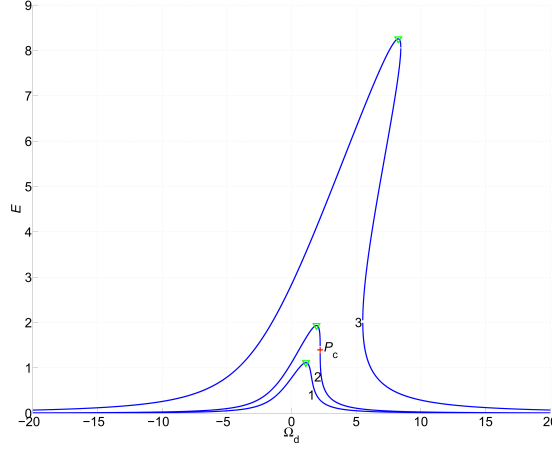
FIG. S2: Bosonization. The steady state value of magnon number expectation value E is calculated as a function of the detuning angular frequency Ω_d by solving the cubic polynomial equation given by Eq. (4) of the main text. Assumed parameters' values are $\gamma_1/\gamma = 0.5$, $\gamma_3/\gamma = 0.1$ and $\omega_K/\gamma = 1$. The driving amplitudes Ω_1 for the curves labelled by the integers 1, 2 and 3 are $0.5\Omega_{1c}$, Ω_{1c} and $10\Omega_{1c}$, respectively, where Ω_{1c} is the value of Ω_1 at the bistability onset point, which is labeled by a red cross symbol. Peak points are labeled by green triangles.

The notation $iW_A/W_b^* = \eta_A e^{i\phi_A}$, where both η_A and ϕ_A are real, allows expressing the gain g_M as

$$g_M = (1 + \eta_A)^2 \cos^2\left(\phi_T + \frac{\phi_A}{2}\right) + (1 - \eta_A)^2 \sin^2\left(\phi_T + \frac{\phi_A}{2}\right)$$
$$= 1 + 2\eta_A \cos\left(2\phi_T + \phi_A\right) + \eta_A^2 \ .$$
$$\text{(S51)}$$

Similarly to the rapid disentanglement model, the steady state response is periodic in the phase ϕ_T with period π [compare to Eq. (S39)].

Consider the case where both ω_A and $\beta_+\beta_-$ are assumed to be sufficiently small to validate an approximation, in which terms of order $O\left(\omega_A^2\right)$ are disregarded, and terms of first order in ω_A are evaluated in the limit $\beta_+\beta_- \to 0$. For this case

$$\eta_A = \left|\frac{W_A}{W_b^*}\right| = \frac{\omega_A \Omega_{L1}}{2\omega_K\sqrt{\Omega_d^2 + \gamma^2}} \ , \tag{S52}$$

and Eq. (S49) yields a cubic polynomial equation for E given by Eq. (4) of the main text.

For any given transverse driving amplitude $\Omega_1 \equiv \omega_{T1}g_M$, the cubic polynomial equation allows calculating the magnon number expectation value E as a function of the angular frequency detuning Ω_d. The plots shown in Fig. S2 demonstrate the transition from the mono–stability $\Omega_1 < \Omega_{1c}$ to the bistability $\Omega_1 > \Omega_{1c}$ regions, where Ω_{1c} is the value of Ω_1 at the bistability onset point (see the red cross symbol in Fig. S2) [S7].

Note that the analysis above is based on the assumption that magnetization is uniform. This simplifying assumption has been employed before to model Kerr nonlinearity in FMSR [S3]. For the more general case, the response of the magnetic medium is decomposed into spin waves [S8]. Note, however, that spin wave theory [S9] is based on the same Bosonization method (i.e. Holstein–Primakoff transformation [S1]) that is employed in this section. As was shown above in section S1, the Heisenberg equations of motion that are derived from the system's Hamiltonian are all linear. Multistability, which is excluded by this linearity, becomes possible when Bosonization is implemented, regardless of whether or not magnetization is assumed to be uniform.

What is the validity range of the assumption that magnetization is uniform? The system's response generally depends on the dispersion relation of spin waves. The effect of exchange interaction on the dispersion relation is characterized by the dimensionless parameter $\epsilon_{ex} = \omega_M \lambda_{ex} k^2/\omega_0$, where $\omega_M = -\gamma_e \mu_0 M_S$, $\gamma_e/2\pi = 28\,\text{GHz}\,\text{T}^{-1}$ is the gyromagnetic ratio, μ_0 is the free space permeability, M_S is the saturated magnetization, λ_{ex} is the exchange constant, $k = 2\pi/\lambda_m$, λ_m is the spin wavelength, and ω_0 is the Larmor angular frequency [see Eq. (5.18) of Ref. [S9]]. For sufficiently small values of the transverse ω_d and longitudinal ω_f detuning angular frequencies, the effect of exchange–induced dispersion can be disregarded [S68]. From the condition $\epsilon_{ex} \simeq 1$ for the case $\lambda_m = R_s$ one
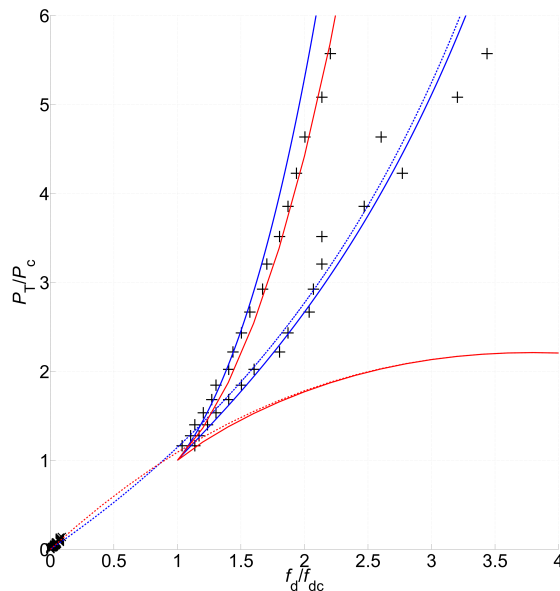
FIG. S3: Bistability. Onset of bistability occurs at driving frequency detuning $f_{\rm d}$ denoted by $f_{\rm dc}$, and driving power $P_{\rm T}$ denoted by $P_{\rm c}$. Measured jump and peak points are labeled by the symbols $+$ and $\times$, respectively. Theoretical predictions derived from the rapid disentanglement and Bosonization–based models are colored by blue and red, respectively. The following measured FMSR parameters are used for the calculations $\omega_0/(2\pi) = 4.062101$ GHz, $P_{\rm c} = 13.5$ dBm, $\gamma_1/\gamma = 0.4$ and $\gamma_3/\omega_{\rm K} = 5.8 \times 10^{-2}$.

finds that exchange–induced dispersion can be approximately disregarded provided that $\max\left(\left|\omega_{\rm d}\right|, \left|\omega_{\rm f}\right|\right) \lesssim \omega_{\rm D}$, where $\omega_{\rm D} = \omega_{\rm M}\lambda_{\rm ex}\left(2\pi/R_{\rm s}\right)^2$. For our experimental setup $\omega_{\rm D}/(2\pi) \simeq 2$ kHz [S9].

S5. BISTABILITY

Both the rapid disentanglement model (see section S3) and the Bosonization–based model (see section S4) predict bistability. The plot in Fig. S3 presents a comparison between experimental mapping of the region of bistability, which is measured with transverse driving only, and theoretical predictions. The experimental mapping is performed by sweeping both transverse driving detuning frequency $f_{\rm d}$ and transverse driving power $P_{\rm T}$, and monitoring FMSR response. Above a critical value of the driving power, which is denoted by $P_{\rm c}$, hysteresis is observed in the dependency on $f_{\rm d}$. The driving detuning frequency $f_{\rm d}$ at the bistability onset point (i.e. for $P_{\rm T} = P_{\rm c}$) is denoted by $f_{\rm dc}$. For any given value of transverse driving power $P_{\rm T}$ in the region of bistability (i.e. for $P_{\rm T} > P_{\rm c}$), the lower (upper) frequency bound of the region of bistability is determined by sweeping $f_{\rm d}$ upwards (downwards), and identifying the driving detuning frequency $f_{\rm d}$ at which the response exhibits a sharp jump. The measured jump points are labelled in Fig. S3 using the symbol $+$. The symbol $\times$ is used to label measured peak points.

Theoretical predictions derived from the rapid disentanglement model are blue colored [see the cubic polynomial equation (S29)], whereas the color red is used for predictions derived from the Bosonization–based model [see the cubic polynomial equation (S49)]. For both models, calculated jump points are represented by solid lines, whereas dashed lines are used for calculated peak points. The data–theory comparison presented in Fig. S3 indicates that the rapid disentanglement model better aligns with the experimental results.

[S1] T Holstein and Hl Primakoff, "Field dependence of the intrinsic domain magnetization of a ferromagnet", *Physical Review*, vol. 58, no. 12, pp. 1098, 1940.

[S2] Robert M Hill and Robert S Bergman, "Nonlinear response of yig", *Journal of Applied Physics*, vol. 32, no. 3, pp. S227–S228, 1961.

[S3] Yi-Pu Wang, Guo-Qiang Zhang, Dengke Zhang, Xiao-Qing Luo, Wei Xiong, Shuai-Peng Wang, Tie-Fu Li, C-M Hu, and JQ You, "Magnon kerr effect in a strongly coupled cavity-magnon system", *Physical Review B*, vol. 94, no. 22, pp. 224410, 2016.

[S4] GuoQiang Zhang, YiPu Wang, and JianQiang You, "Theory of the magnon kerr effect in cavity magnonics", *SCIENCE CHINA Physics, Mechanics & Astronomy*, vol. 62, no. 8, pp. 987511, 2019.

[S5] Cijy Mathai, Sergei Masis, Oleg Shtempluck, Shay Hacohen-Gourgy, and Eyal Buks, "Frequency mixing in a ferrimagnetic sphere resonator", *Euro. Phys. Lett.*, vol. 131, 2020.

[S6] C. W. Gardiner and M. J. Collett, "Input and output in damped quantum systems: Quantum stochastic differential equations and the master equation", *Phys. Rev. A*, vol. 31, pp. 3761, 1985.

[S7] Bernard Yurke and Eyal Buks, "Performance of cavity-parametric amplifiers, employing kerr nonlinearites, in the presence of two-photon loss", *J. Lightwave Tech.*, vol. 24, pp. 5054–5066, 2006.

[S8] Suhl, H, "The theory of ferromagnetic resonance at high signal powers", *Journal of Physics and Chemistry of Solids*, vol. 1, pp. 209–227, 1957.

[S9] Stancil, Daniel D and Prabhakar, Anil, "Spin waves", *Springer*, 2009.